Electronic Supplementary Information for

Ratiometric Oxygen Sensors of Cyclometalated Iridium(III) with Enhanced Quantum Yields and Variable Dynamic Ranges

Gregory D. Sutton, Chenggang Jiang, Gardenia Liu, and Thomas S. Teets*

Department of Chemistry, University of Houston,
3585 Cullen Blvd. Room 112, Houston, TX 77204-5003, USA
email: tteets@uh.edu

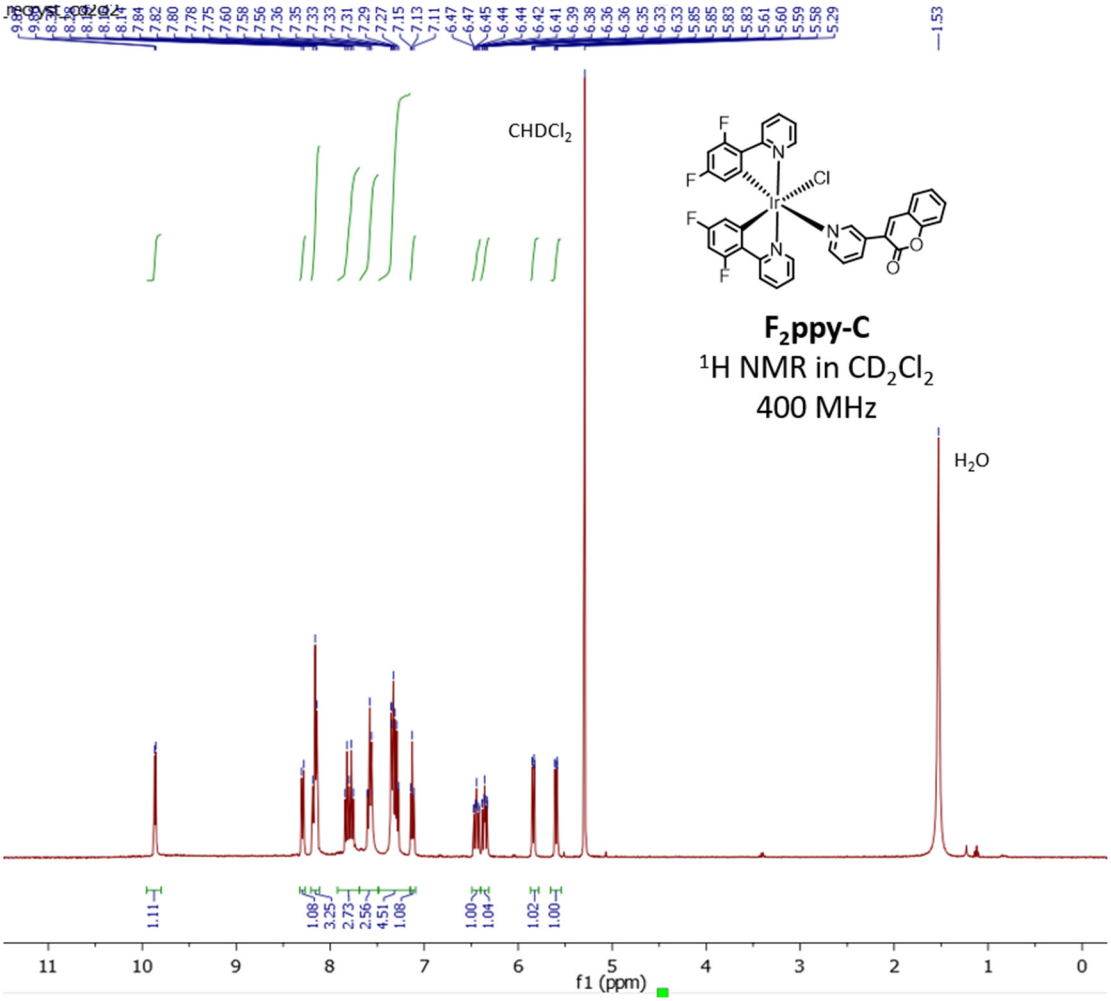

Fig. S1. ^{1}H NMR spectrum of complex **F$_2$ppy-C** recorded at 400 MHz in CD_2Cl_2.

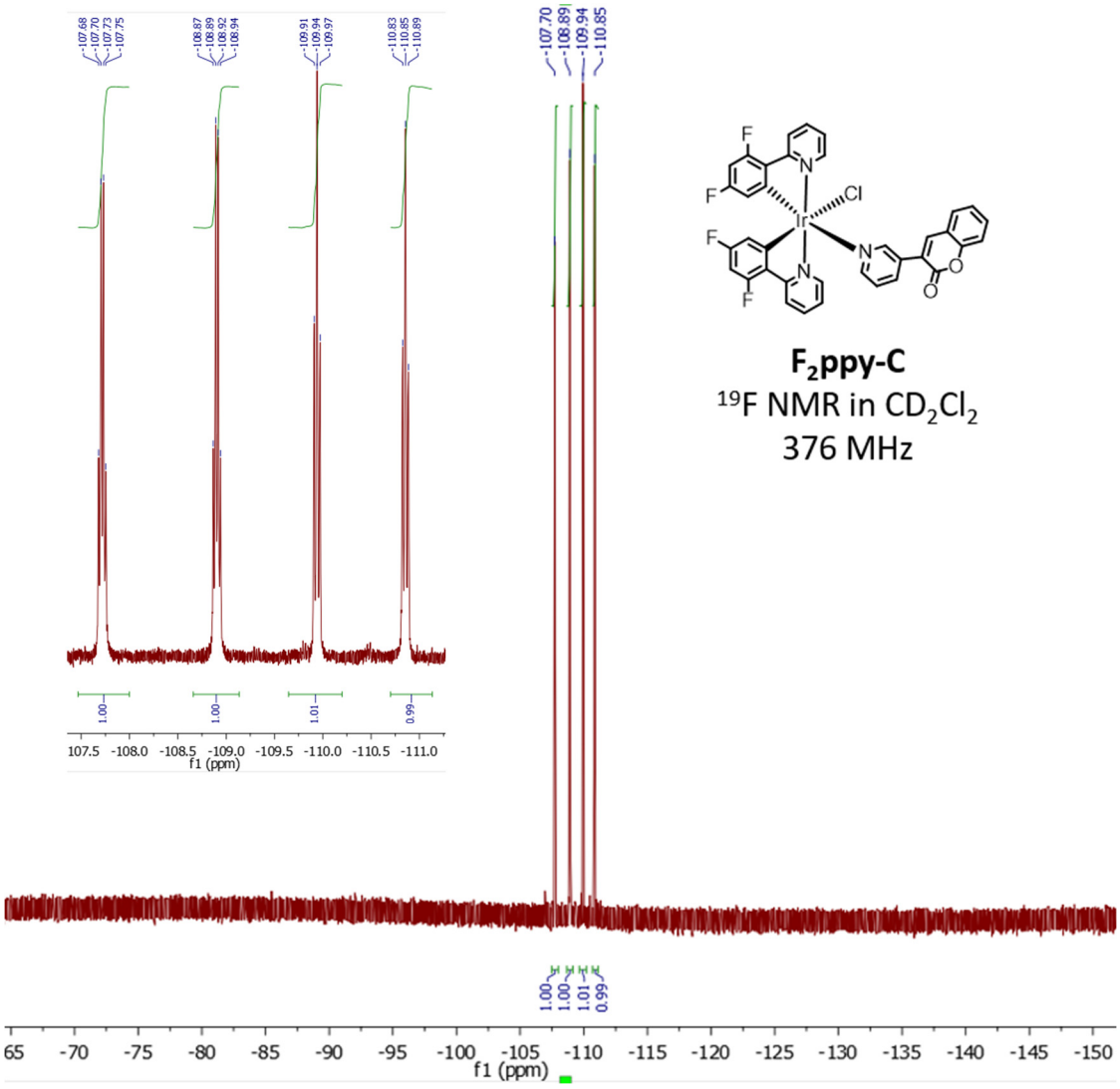

Fig. S2. ^{19}F NMR spectrum of **F$_2$ppy-C** recorded at 376 MHz in CD_2Cl_2.

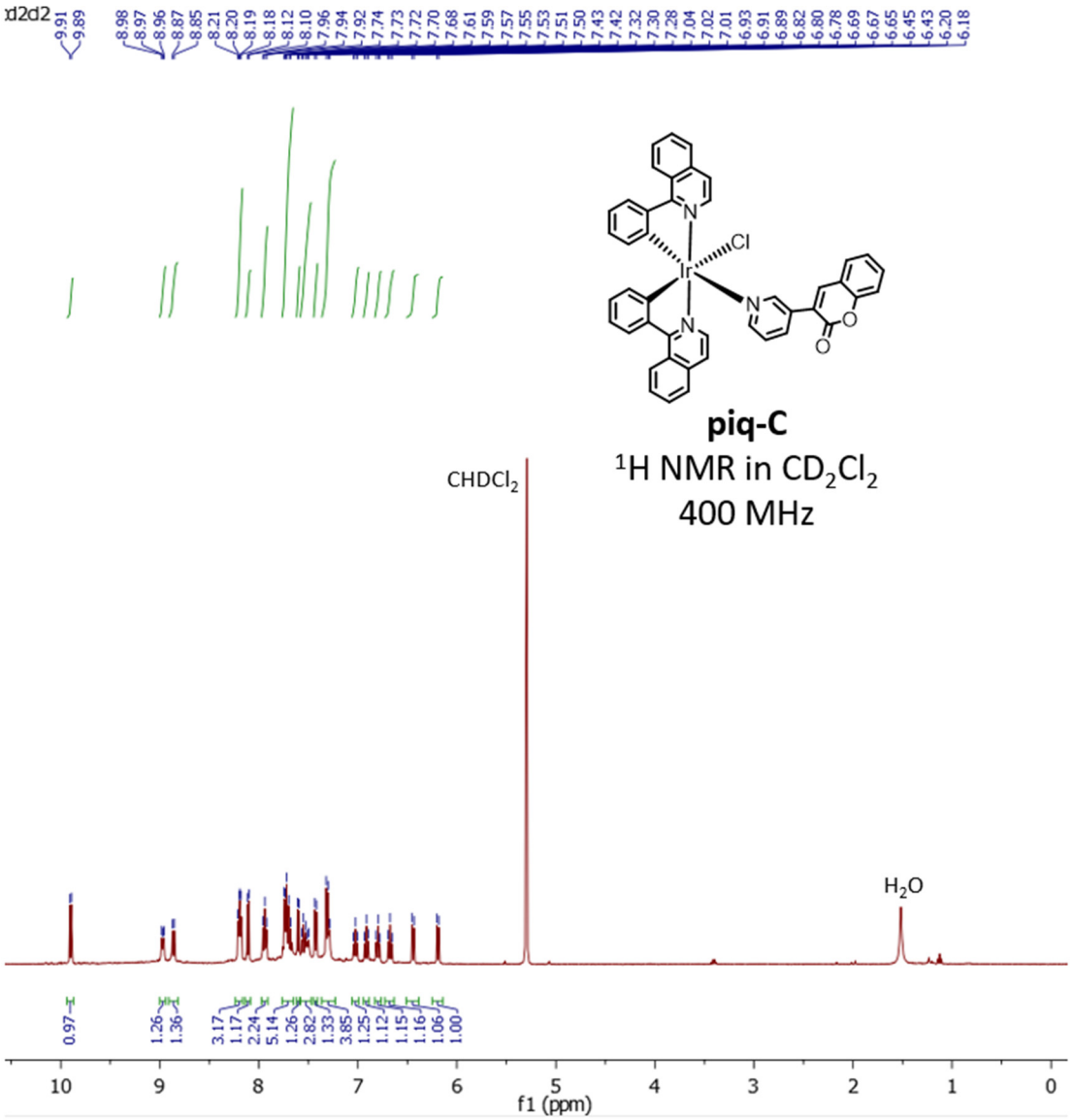

Fig. S3. ^{1}H NMR spectrum of **piq-C** recorded at 400 MHz in CD_2Cl_2.

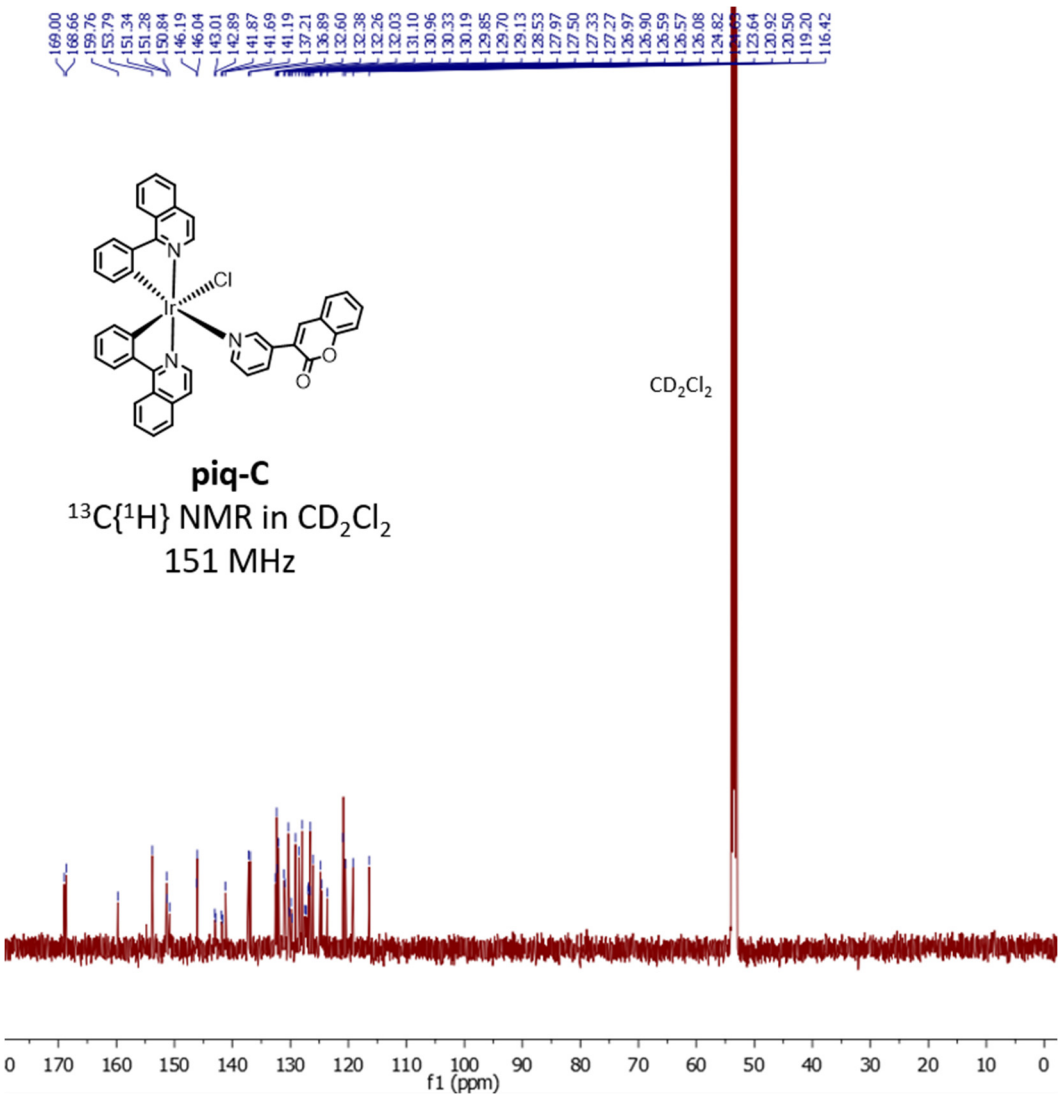

Fig. S4. $^{13}C\{^{1}H\}$ NMR spectrum of **piq-C** recorded at 151 MHz in CD_2Cl_2.

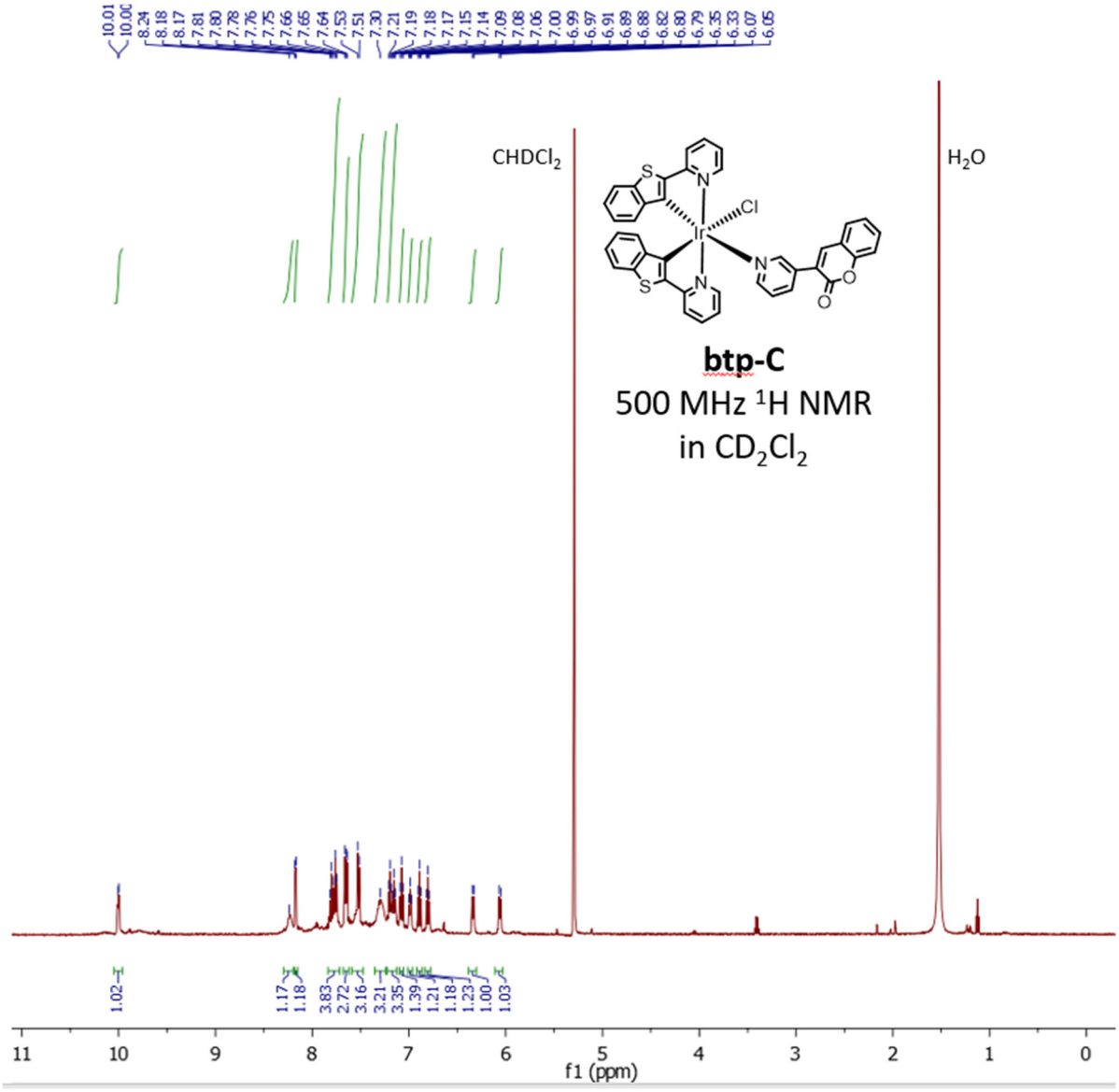

Fig. S5. ^{1}H NMR spectrum of **btp-C** recorded at 500 MHz in CD_2Cl_2.

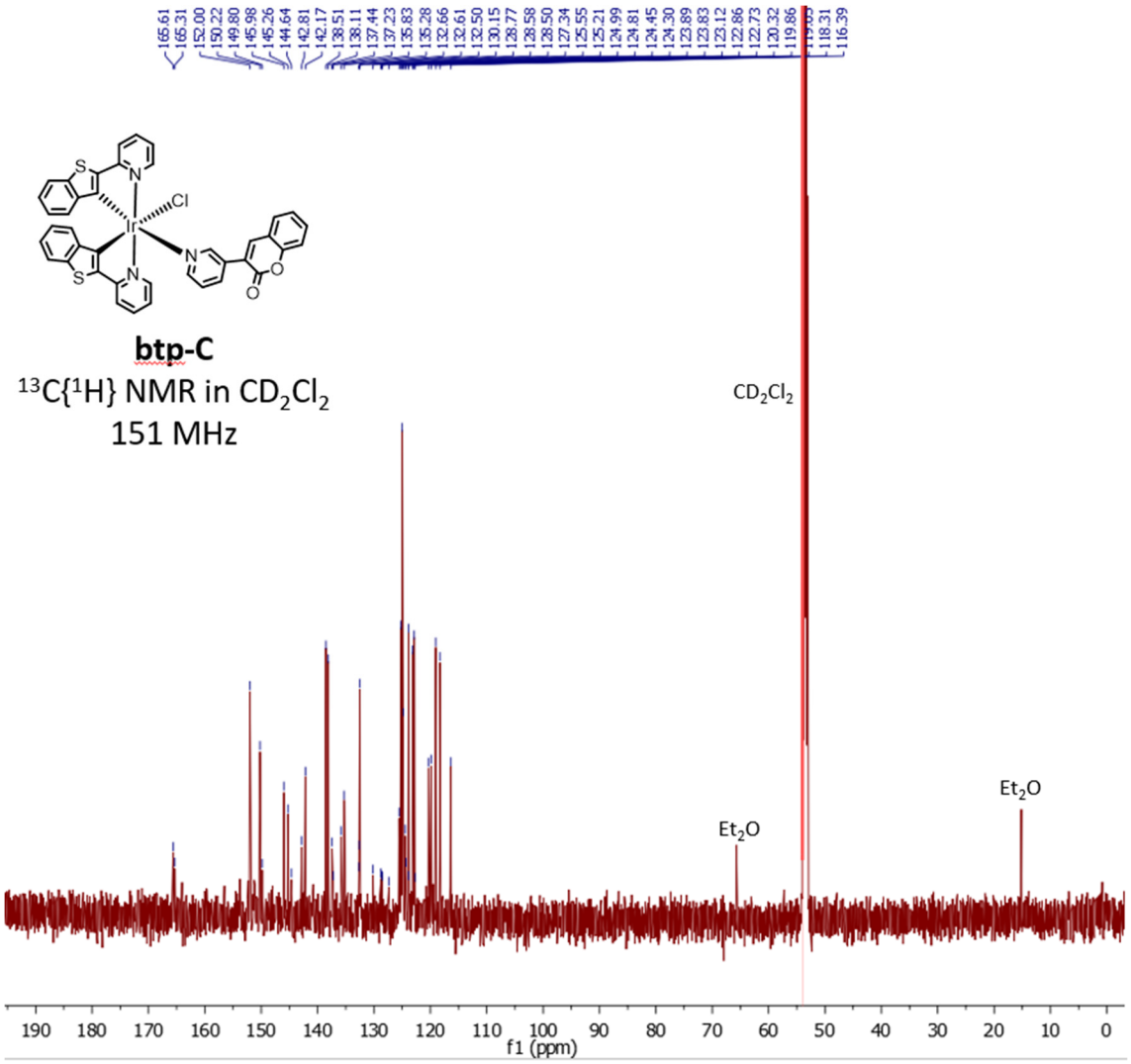

Fig. S6. $^{13}C\{^{1}H\}$ NMR spectrum of **btp-C** recorded at 151 MHz in CD_2Cl_2.

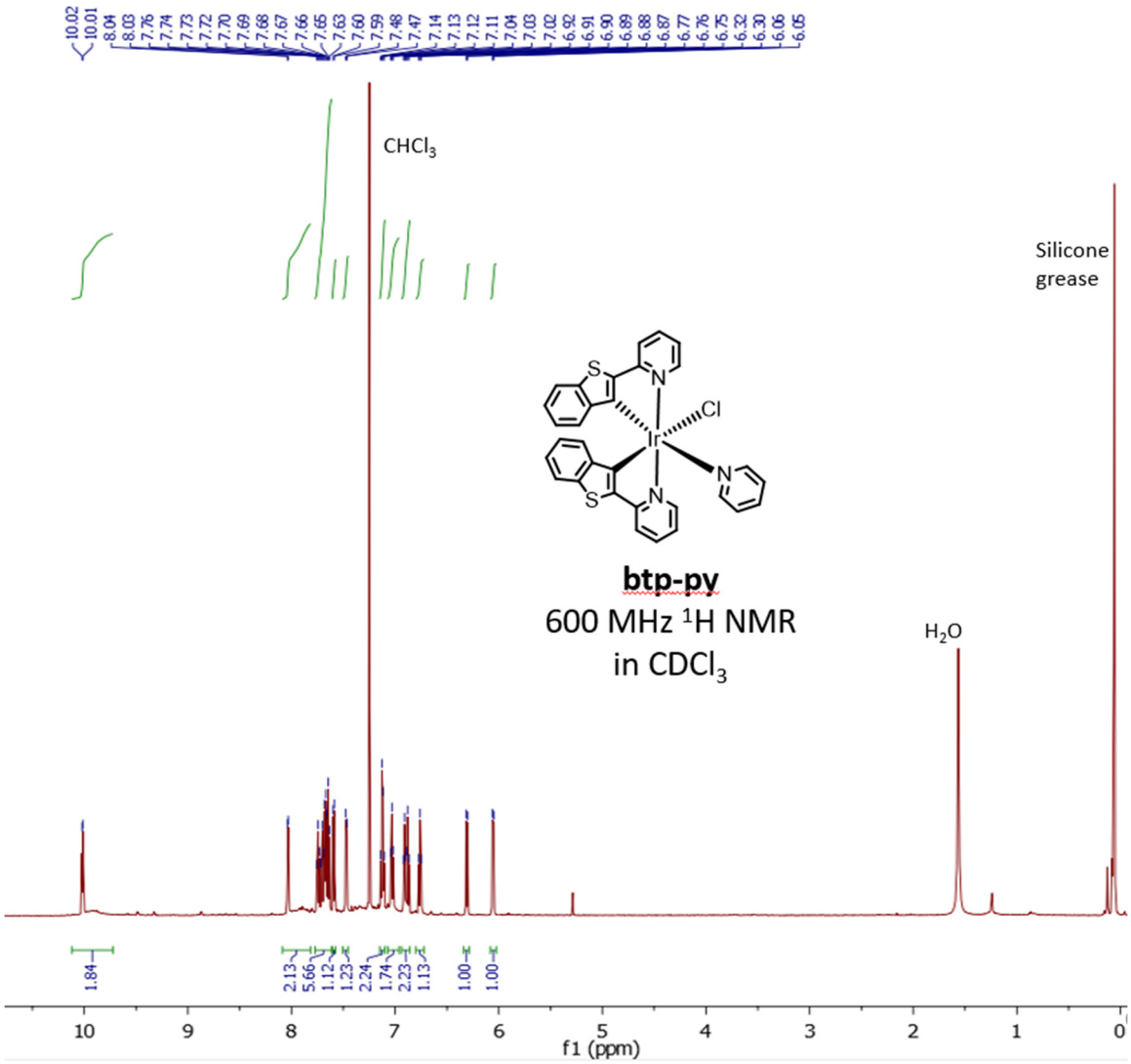

Fig. S7. ^{1}H NMR spectrum of **btp-py** recorded at 600 MHz in $CDCl_3$.

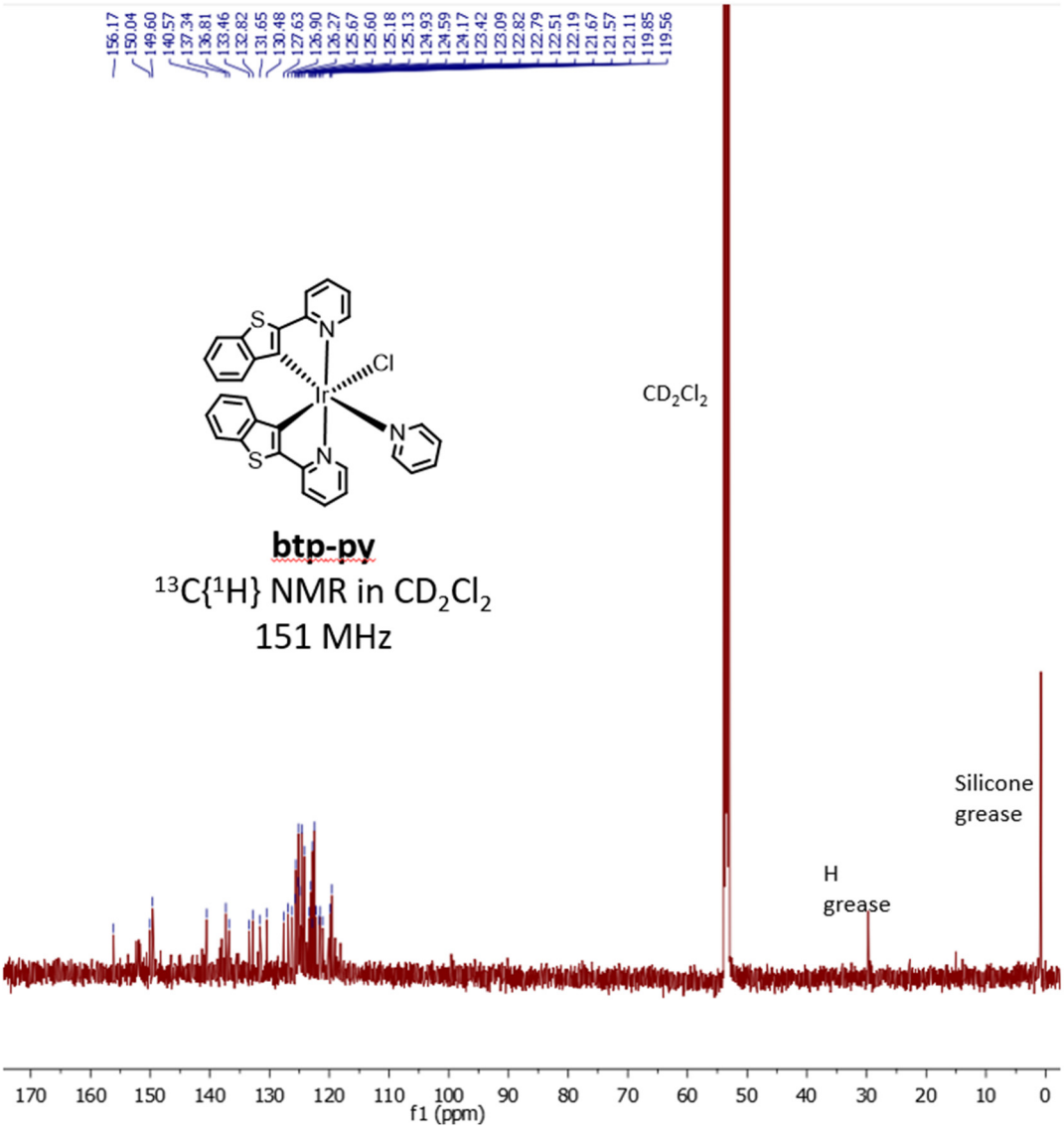

Fig. S8. $^{13}C\{^{1}H\}$ NMR spectrum of **btp-py** recorded at 151 MHz in CD_2Cl_2.

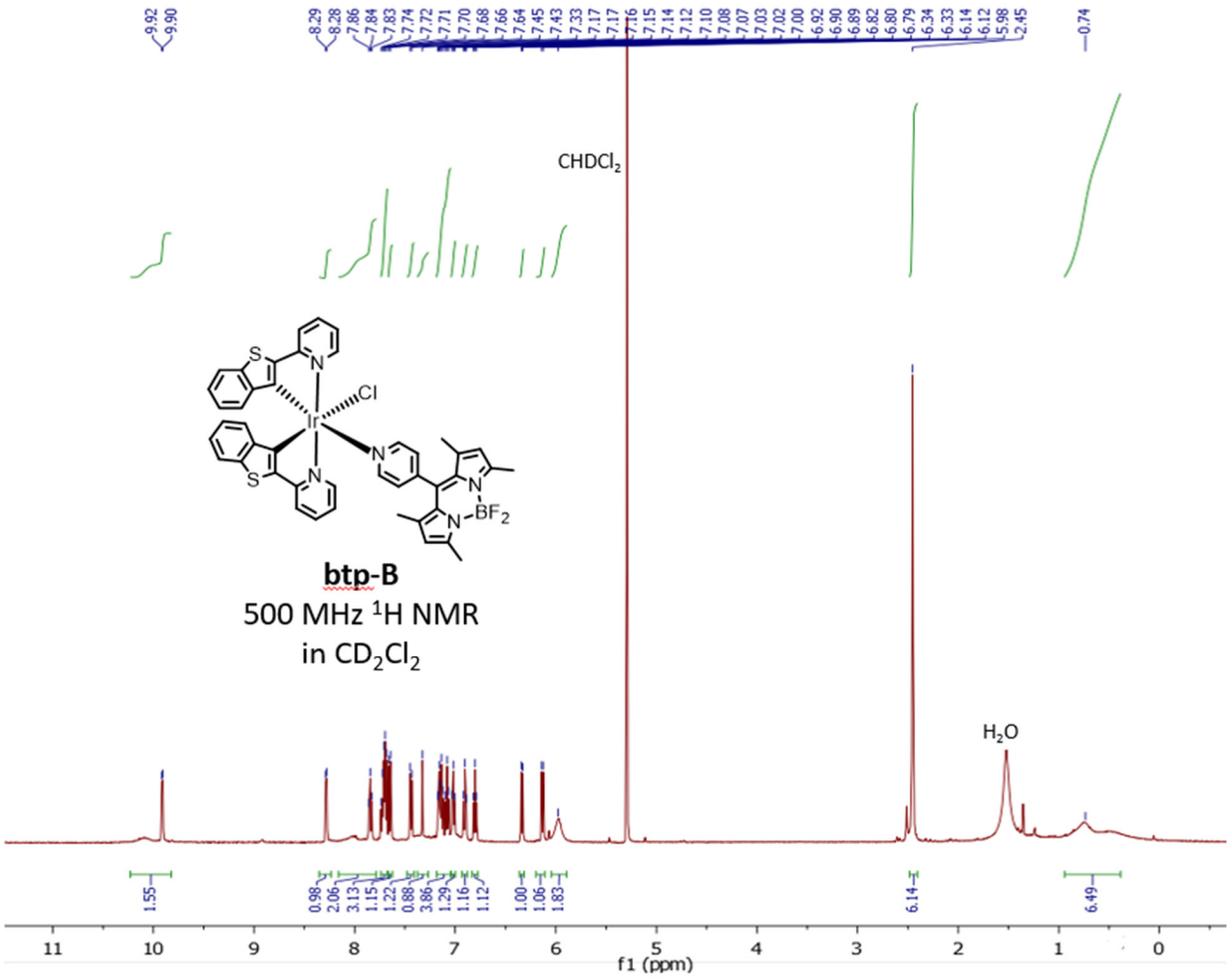

Fig. S9. ^{1}H NMR spectrum of **btp-B** recorded at 500 MHz in CD_2Cl_2.

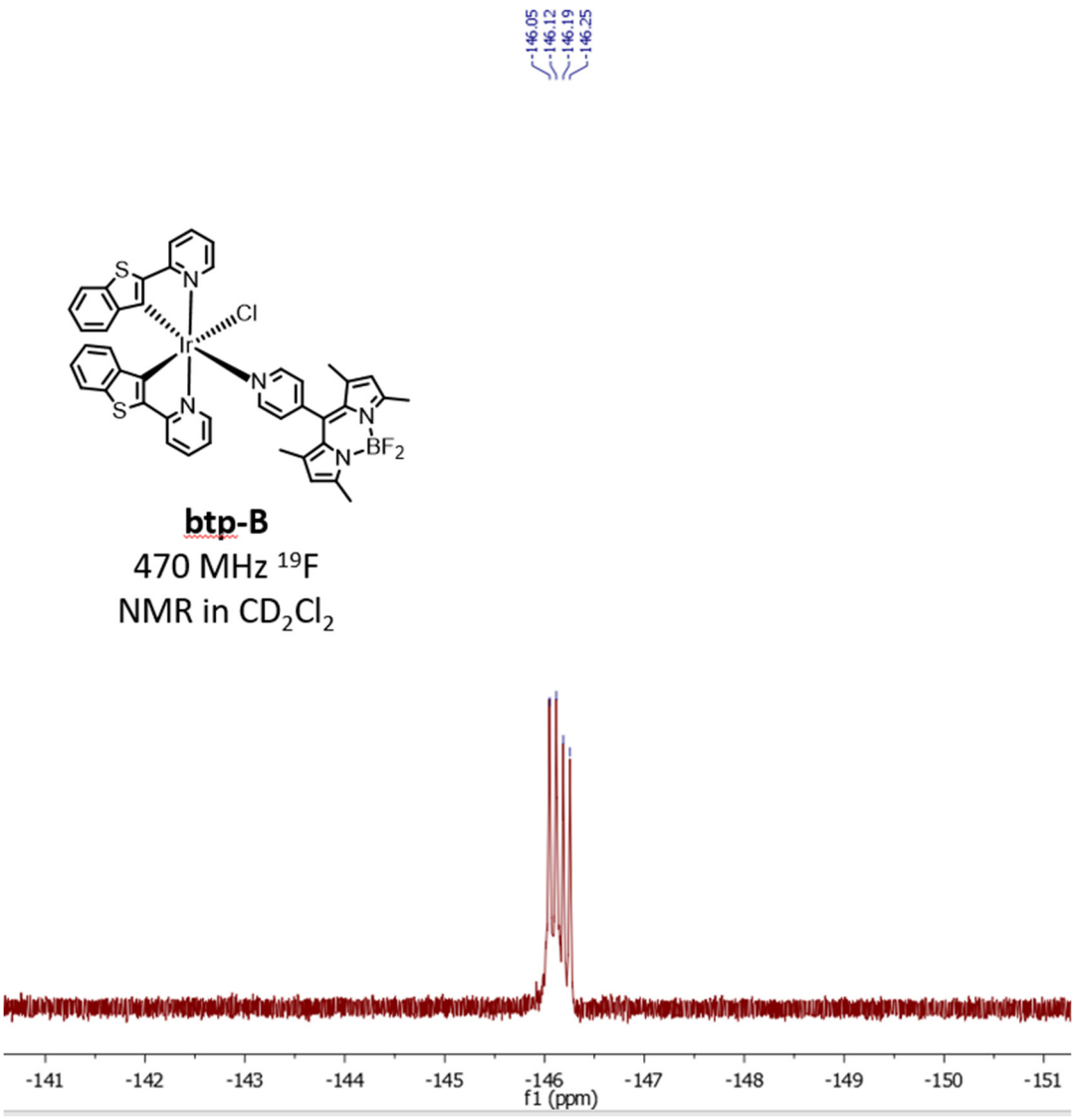

Fig. S10. ^{19}F NMR spectrum of **btp-B** recorded at 470 MHz in CD_2Cl_2.

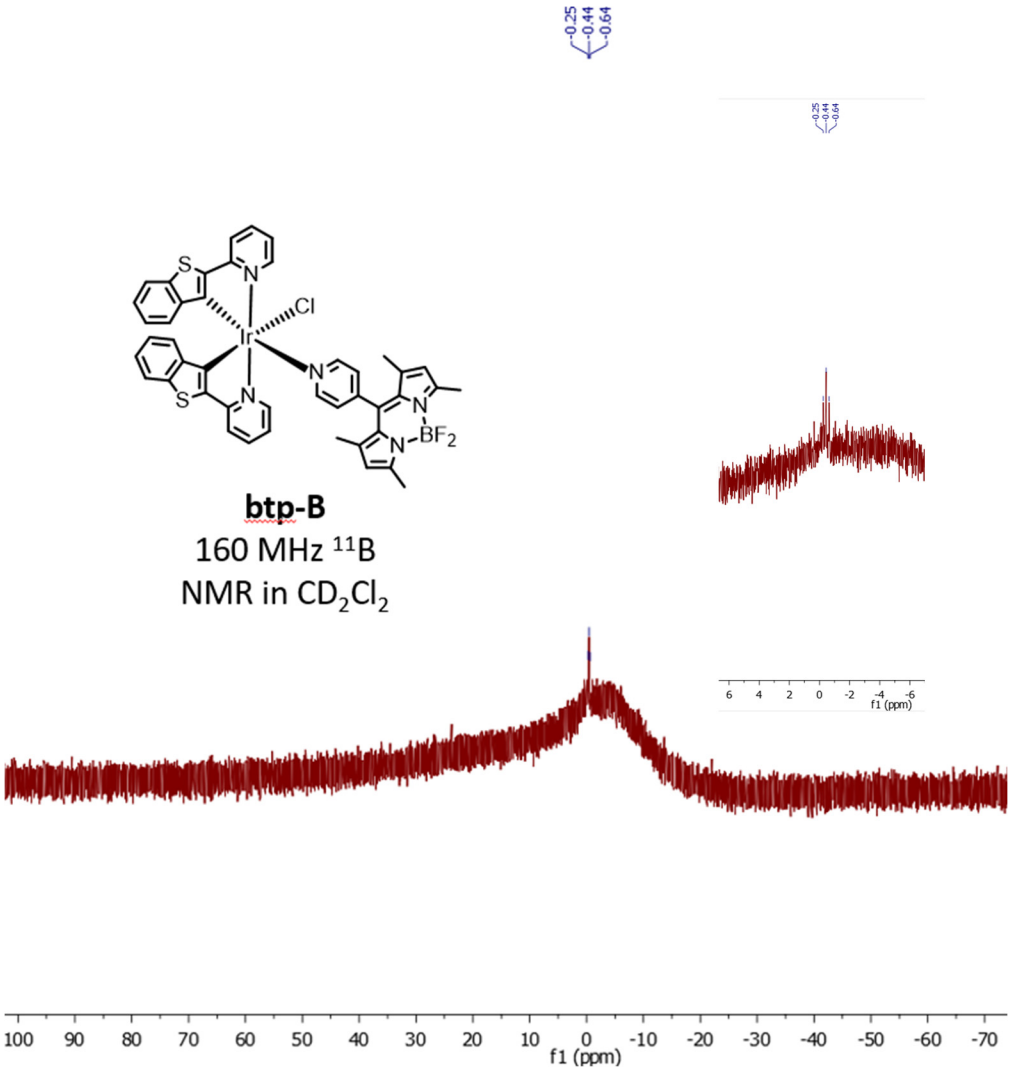

Fig. S11. ^{11}B NMR spectrum of **btp-B** recorded at 160 MHz in CD_2Cl_2.

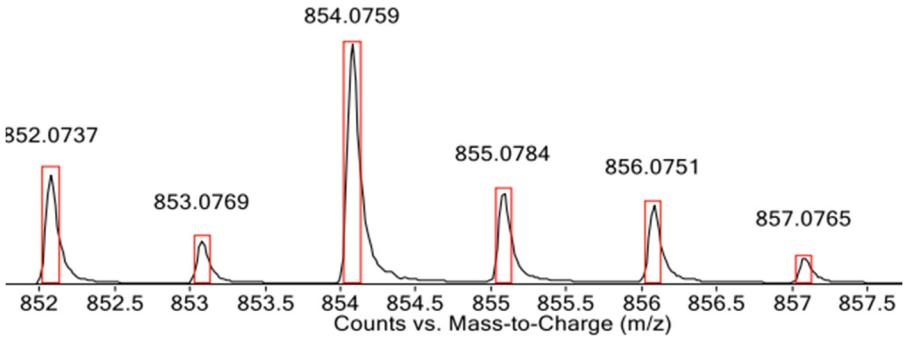

Fig. S12. Simulated (red boxes) and experimental (black peaks) ESI-MS data for complex **F_2ppy-C**, showing the isotropic distribution pattern for the molecular ion peak ($[M + Na]^+$).

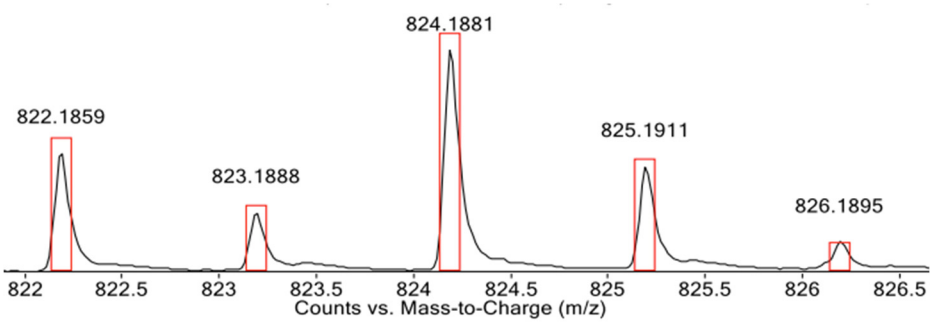

Fig. S13. Simulated (red boxes) and experimental (black peaks) ESI-MS data for complex **piq-C**, showing the isotropic distribution pattern for the molecular ion peak ($[M - Cl]^+$).

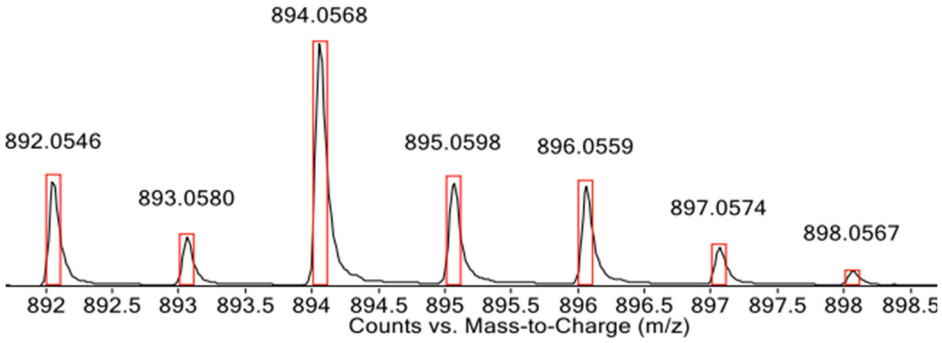

Fig. S14. Simulated (red boxes) and experimental (black peaks) ESI-MS data for complex **btp-C**, showing the isotropic distribution pattern for the peak ($[M + Na]^+$).

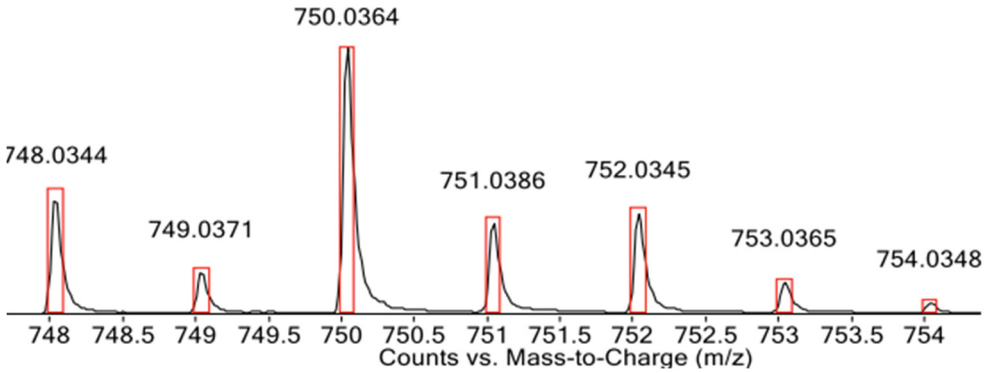

Fig. S15. Simulated (red boxes) and experimental (black peaks) ESI-MS data for complex **btp-py**, showing the isotropic distribution pattern for the molecular ion peak ($[M + Na]^+$).

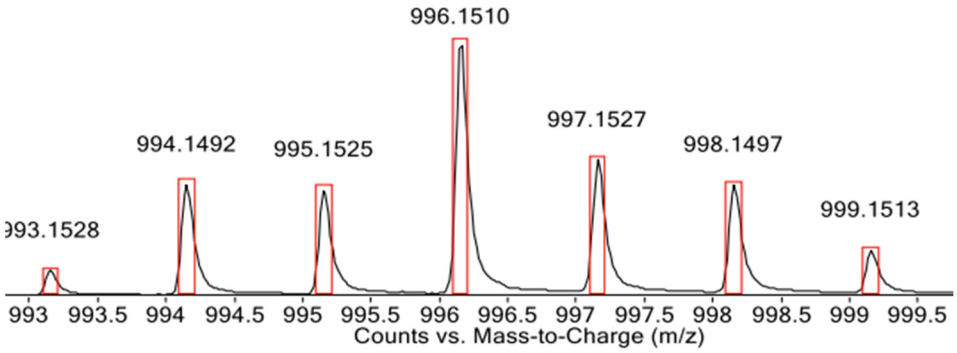

Fig. S16. Simulated (red boxes) and experimental (black peaks) ESI-MS data for complex **btp-B**, showing the isotropic distribution pattern for the peak ($[M + Na]^+$).

Table S1. Summary of X-ray crystallographic data for **btp-py** and **btp-B**.

	btp-py	**btp-B**•$2C_6H_6$
CCDC	2215267	2215268
Crystal data		
Chemical formula	$C_{31}H_{21}ClIrN_3S_2$	$C_{56}H_{46}BClF_2IrN_5S_2$
M_r	727.28	1129.56
Crystal system, space group	Monoclinic, *C*2/*c*	Triclinic, $P\bar{1}$
a, *b*, *c* (Å)	35.543(8), 9.543(2), 16.994(4)	10.1377(11), 15.1859(17), 18.717(2)
α, β, γ (°)	90, 114.027(3), 90	98.632(1), 103.297(1), 100.196(1)
V (Å^3)	5265(2)	2704.7(5)
Z	8	2
μ (mm^{-1})	5.36	2.64
Crystal size (mm)	0.20 × 0.13 × 0.12	0.33 × 0.25 × 0.17
Data collection		
Absorption correction	Empirical (using intensity measurements) *SADABS*	Multi-scan *SADABS*
T_{min}, T_{max}	0.436, 0.746	0.607, 0.746
No. of measured, independent and observed [$I > 2\sigma(I)$] reflections	25793, 5791, 5024	77072, 12477, 11086
R_{int}	0.066	0.063
$(\sin\theta/\lambda)_{max}$ (Å^{-1})	0.641	0.651
Refinement		
$R[F^2 > 2\sigma(F^2)]$, $wR(F^2)$, *S*	0.050, 0.137, 1.02	0.030, 0.084, 1.08
No. of reflections	5791	12477
No. of parameters	343	618
No. of restraints	0	228
$\Delta\rho_{max}$, $\Delta\rho_{min}$ (e Å^{-3})	5.81, -3.36	1.96, -0.73

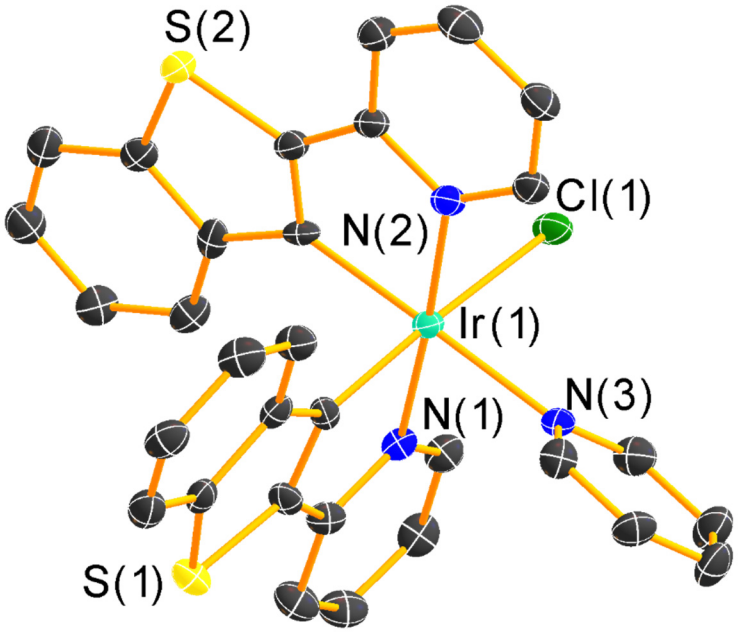

Fig. S17. Molecular structures of **btp-py** determined by single-crystal X-ray diffraction. Thermal ellipsoids are drawn at the 50% probability level with hydrogen atoms omitted.

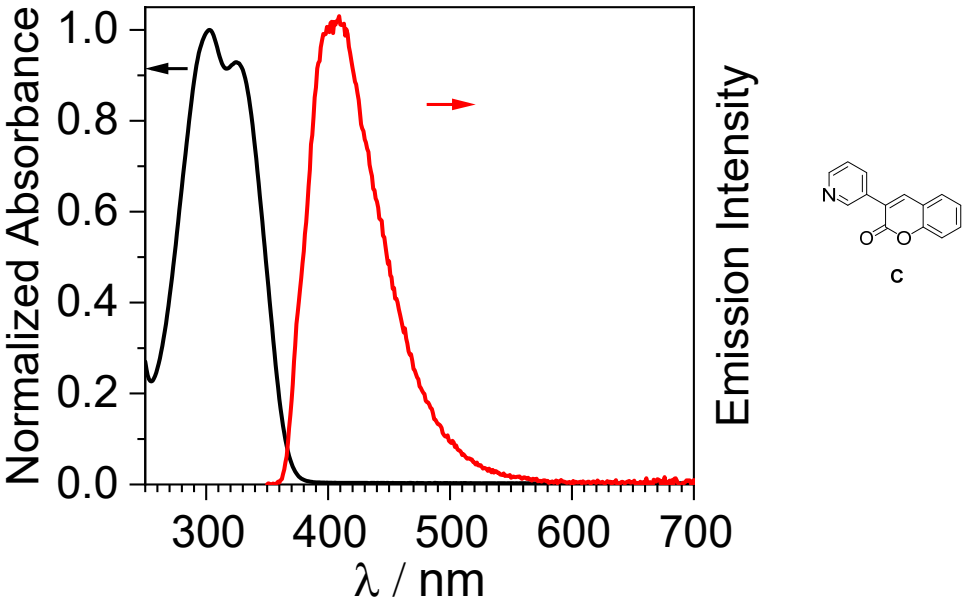

Fig. S18. Overlaid UV-vis absorption (solid black line) and photoluminescence (solid red line) spectra of coumarin **C**, recorded at 293 K in CH_2Cl_2. These data were previously reported.[2]

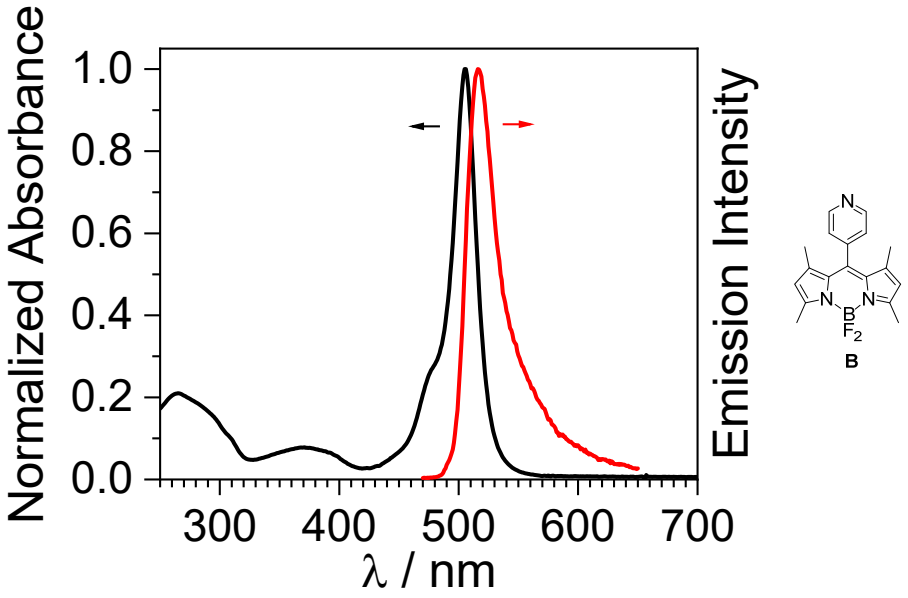

Fig. S19. Overlaid UV-vis absorption (black dashed line) and photoluminescence (red solid line) spectra of BODIPY **B**, recorded at 293 K in CH_2Cl_2. These data were previously reported.[3]

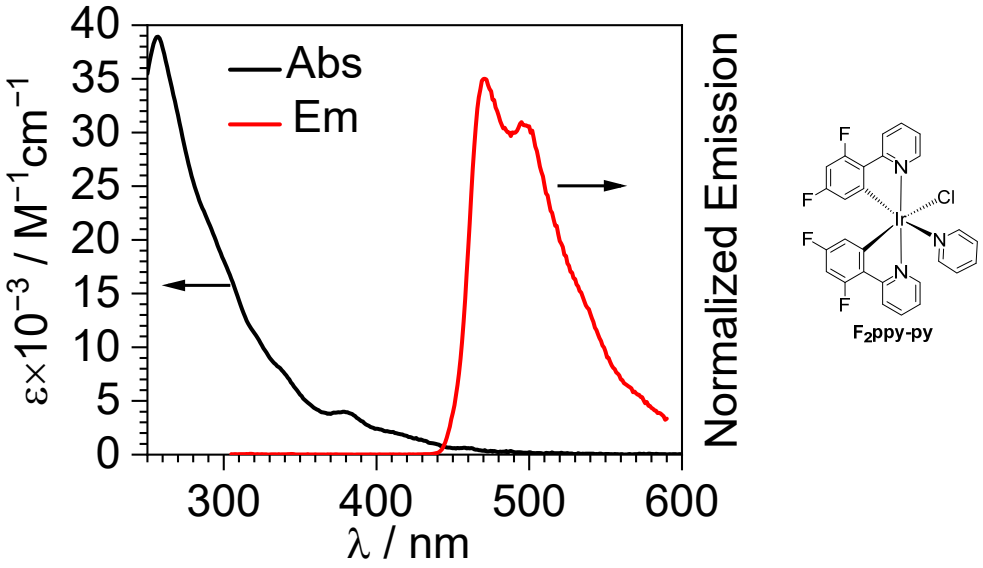

Fig. S20. Overlaid UV-vis absorption (solid black line) and photoluminescence (solid red line) spectra of the pyridine model complex **F_2ppy-py**, recorded in CH_2Cl_2 at 293 K. These data were previously reported.[7]

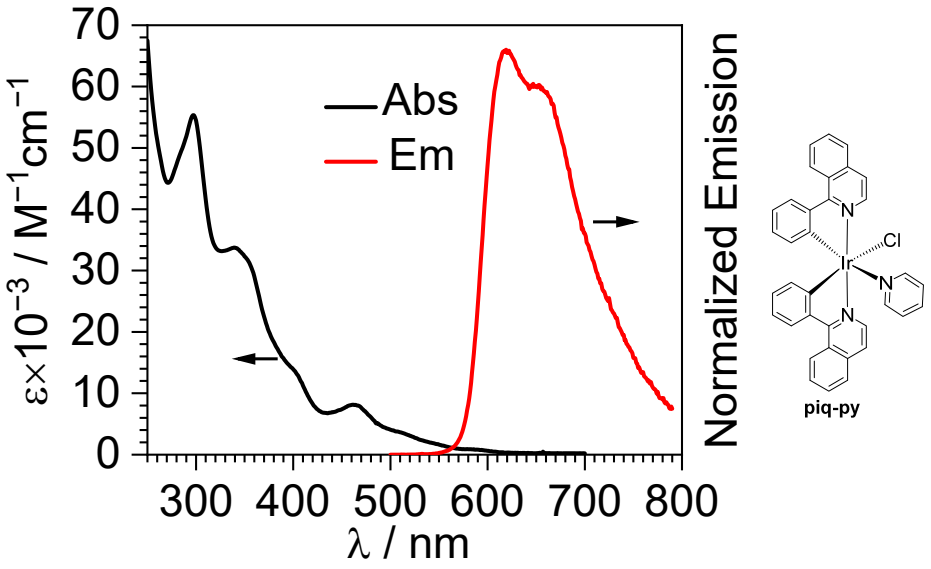

Fig. S21. Overlaid UV-vis absorption (solid black line) and photoluminescence (solid red line) spectra of the pyridine model complex **piq-py**, recorded in CH_2Cl_2 at 293 K. These data were previously reported.[7]

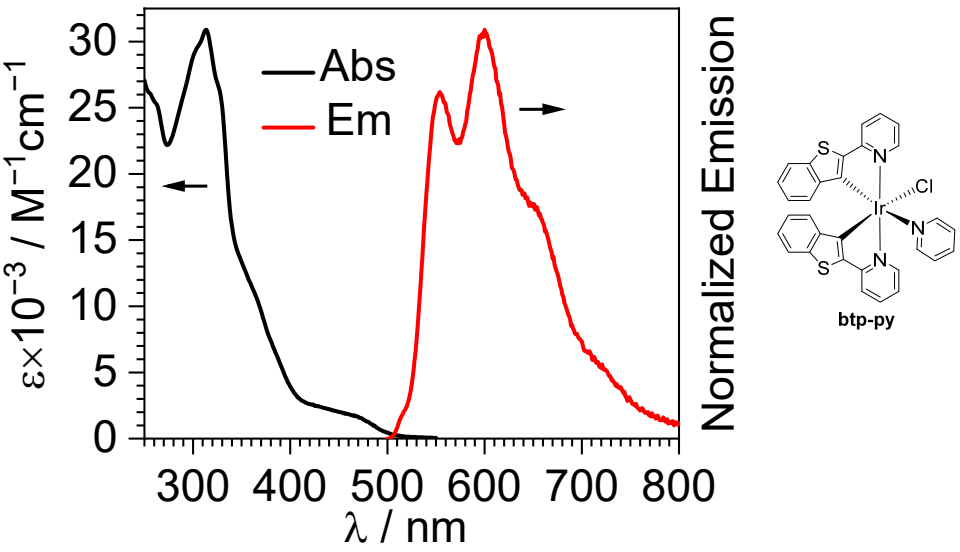

Fig. S22. Overlaid UV-vis absorption (solid black line) and photoluminescence (solid red line) spectra of the pyridine model complex **btp-py**, recorded in CH_2Cl_2 at 293 K.

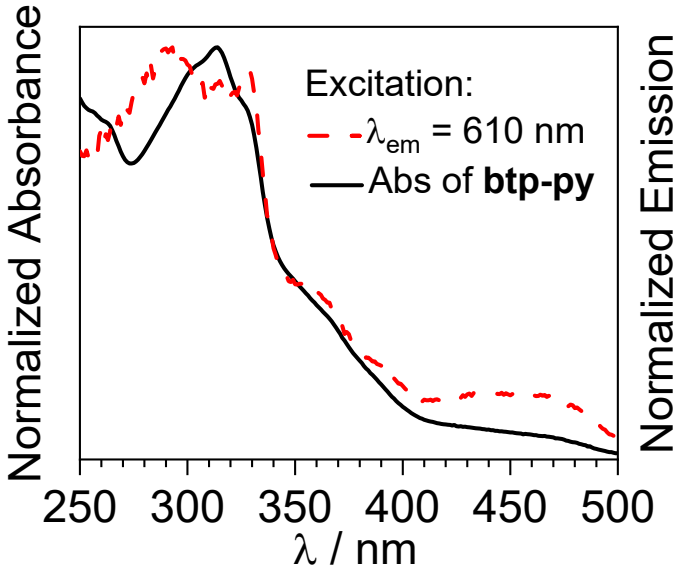

Fig. S23. Overlaid UV-vis absorption (black solid line) and excitation (red dashed line) spectra of **btp-py**. The excitation spectrum was monitored at the peak phosphorescence wavelength.

Table S2. Summary of photoluminescence data for the free coumarin and BODIPY fluorophores and the pyridine-terminated iridium model complexes. Recorded in CH_2Cl_2 at room temperature.

Compound	Reference	λ_{em}/nm (293 K)	Φ_{PL}	τ_{PL}
C	[2]	406	0.083	3.4 ns
B	[3]	521	0.30	1.9 ns
F₂ppy-py	[7]	470^{max}, 500(sh), 542(sh)	0.06	3.5 µs
piq-py	[7]	619^{max}, 659(sh)	0.29	2.3 µs
btp-py	*this work*	554, 600^{max}, 653	0.13	1.8 µs

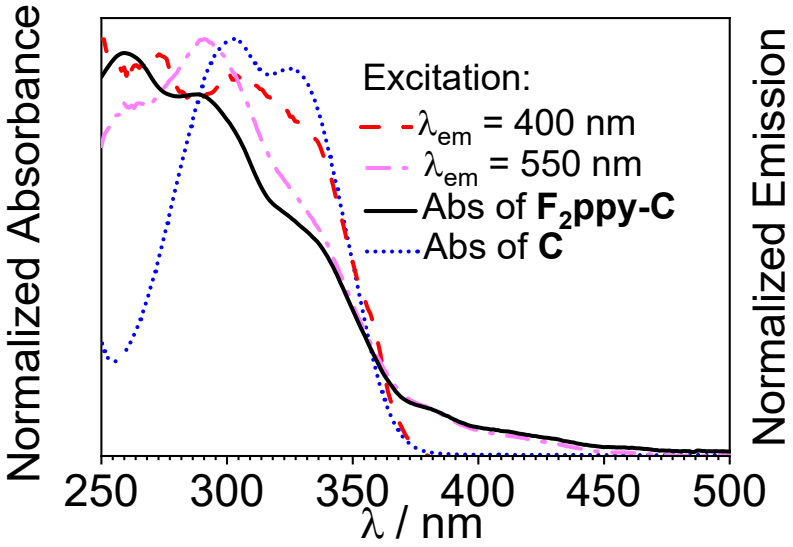

Fig. S24. Overlaid UV-vis absorption (black solid line) and excitation spectra of **F₂ppy-C**. Excitation spectra were monitored at the peak fluorescence (red dashed line) and phosphorescence (magenta dash-dot line) wavelengths. The UV-vis absorption spectrum of coumarin **C** (blue dotted line) is included for reference.

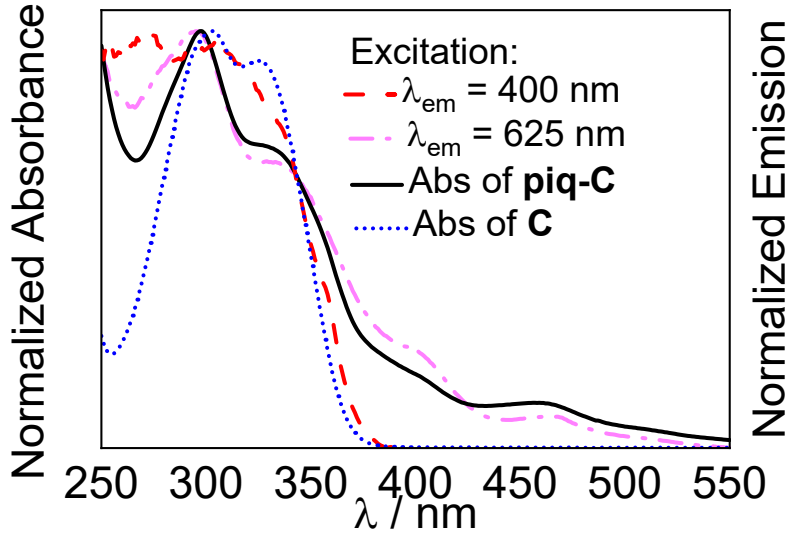

Fig. S25. Overlaid UV-vis absorption (black solid line) and excitation spectra of **piq-C**. Excitation spectra were monitored at the peak fluorescence (red dashed line) and phosphorescence (magenta dash-dot line) wavelengths. The UV-vis absorption spectrum of coumarin **C** (blue dotted line) is included for reference.

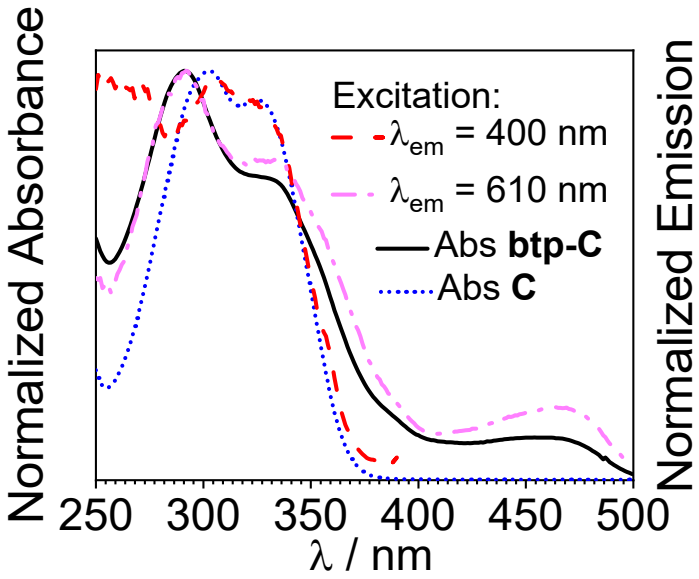

Fig. S26. Overlaid UV-vis absorption (black solid line) and excitation spectra of **btp-C**. Excitation spectra were monitored at the peak fluorescence (red dashed line) and phosphorescence (magenta dash-dot line) wavelengths. The UV-vis absorption spectrum of coumarin **C** (blue dotted line) is included for reference.

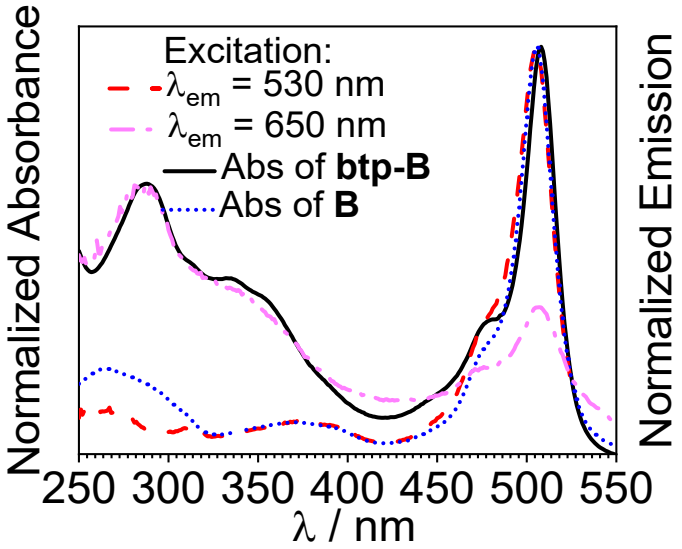

Fig. S27. Overlaid UV-vis absorption (black solid line) and excitation spectra of **btp-B**. Excitation spectra were monitored at the peak fluorescence (red dashed line) and phosphorescence (magenta dash-dot line) wavelengths. The UV-vis absorption spectrum of BODIPY **B** (blue dotted line) is included for reference.

$$\frac{\tau_0}{\tau} = 1 + K_{SV} pO_2 = 1 + k_q \tau_0 pO_2 \quad \text{(S1)}$$

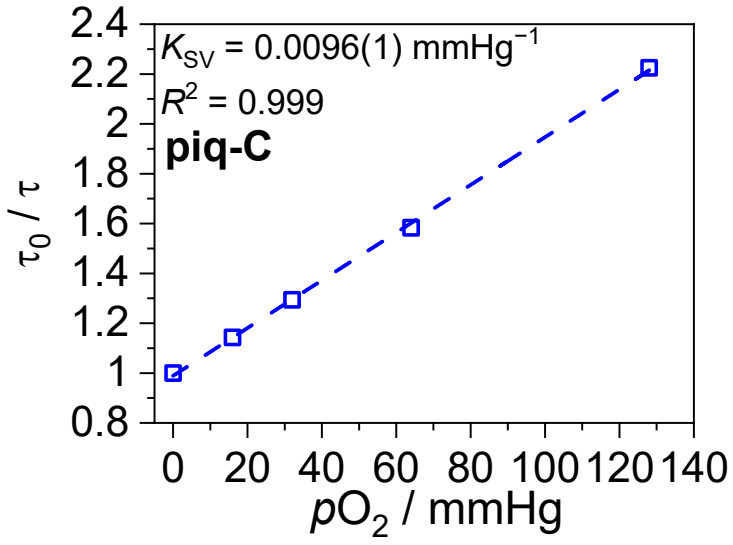

Fig. S28. Stern-Volmer plot of **piq-C** determined using the lifetime method (Equation S2). The y-axis of τ_0 / τ denotes the ratio of the lifetime in the absence of oxygen (τ_0) to the lifetime in the presence of oxygen (τ). The parenthetical number in K_{SV} represents the error in the fit for the last reported digit, and the R^2 value is also provided.

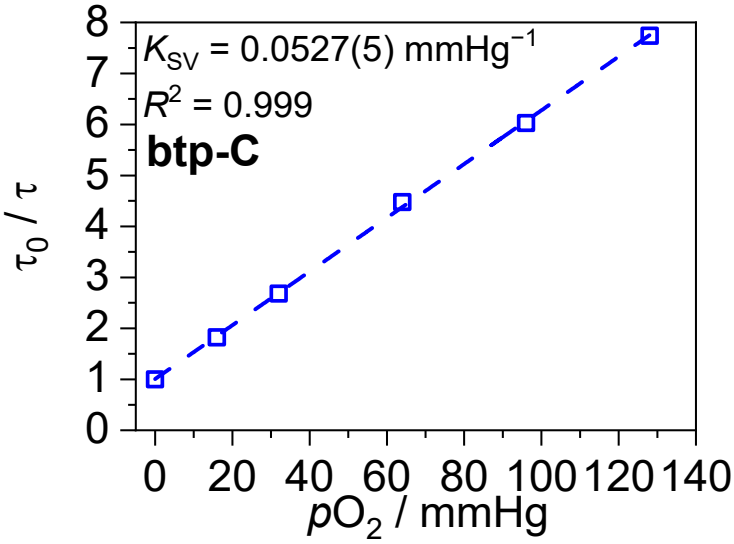

Fig. S29. Stern-Volmer plot of **btp-C** determined using the lifetime method (Equation S2). The y-axis of τ_0 / τ denotes the ratio of the lifetime in the absence of oxygen (τ_0) to the lifetime in the presence of oxygen (τ). The parenthetical digit in K_{SV} represents the error in the fit for the last reported digit, and the R^2 value is also provided.

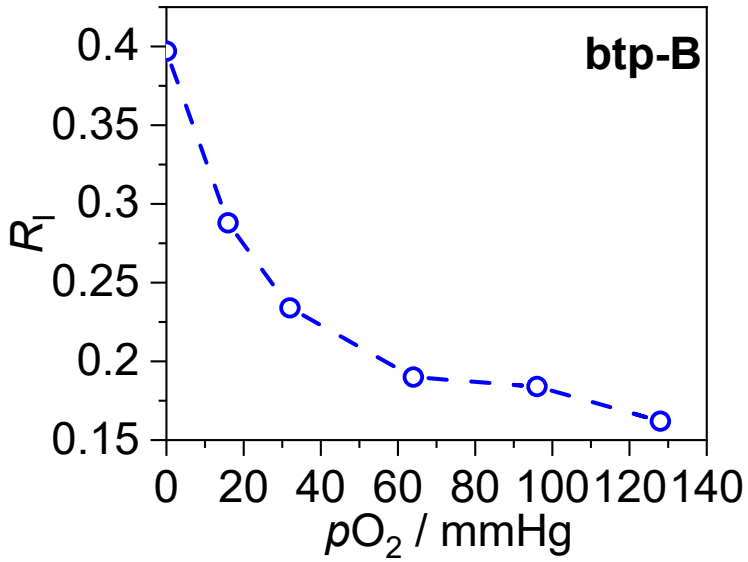

Fig. S30. Ratiometric response of complex **btp-B** as a function of oxygen partial pressure. The dotted line is drawn simply as a guide, and the ratio was determined from the emission signals at the peak wavelengths for phosphorescence (603 nm) and fluorescence (524 nm).

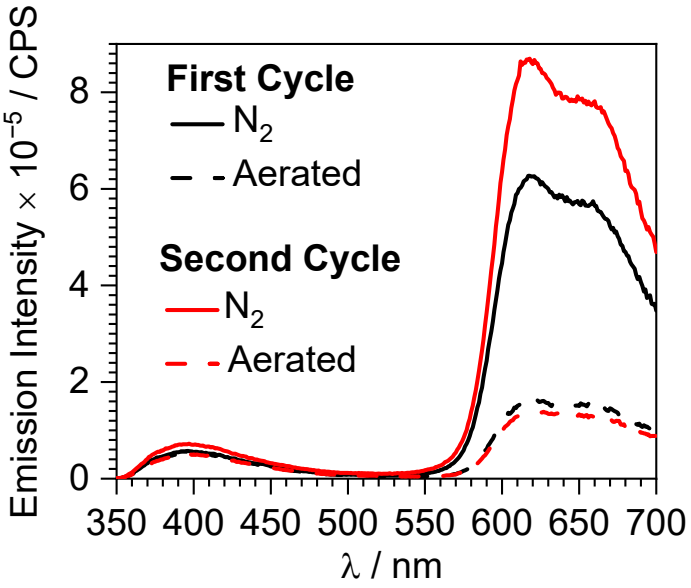

Fig. S31. Photoluminescence spectra of **piq-C** with repeated cycling of N_2 and aerobic atmospheres. 1) The initial N_2-saturated sample was prepared in a nitrogen-filled glovebox using deoxygenated CH_2Cl_2. 2) The sample was then exposed to air to obtain the aerated spectrum. 3) The aerated sample was deaerated with three freeze-pump-thaw cycles on a Schlenk line, and then added back into the cuvette in the glovebox. This process was repeated to get a total of two cycles.

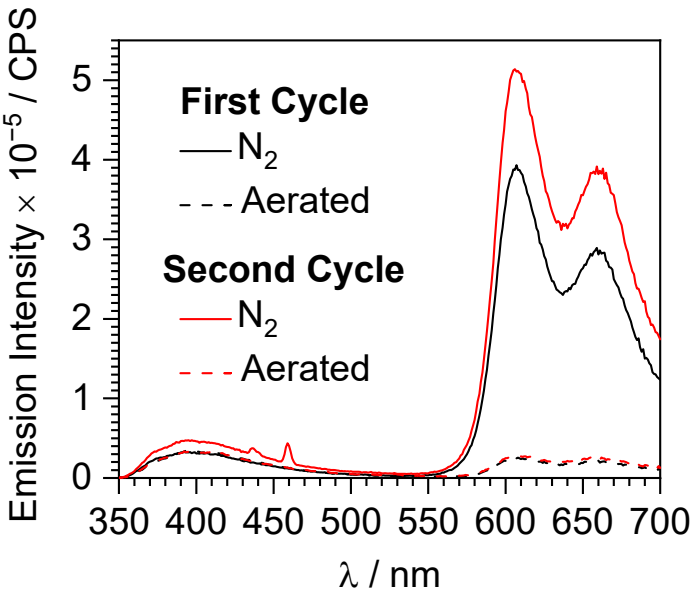

Fig. S32. Photoluminescence spectra of **btp-C** with repeated cycling of N_2 and aerobic atmospheres. 1) The initial N_2-saturated sample was prepared in a nitrogen-filled glovebox using deoxygenated CH_2Cl_2. 2) The sample was then exposed to air to obtain the aerated spectrum. 3) The aerated sample was deaerated with three freeze-pump-thaw cycles on a Schlenk line, and then added back into the cuvette in the glovebox. This process was repeated to get a total of two cycles.

ESI References

1 M. Nonoyama, *Bull. Chem. Soc. Jpn.*, 1974, **47**, 767–768.
2 Y. Wu, G. D. Sutton, M. D. S. Halamicek, X. Xing, J. Bao and T. S. Teets, *Chem. Sci.*, 2022, **13**, 8804–8812.
3 K. S. Choung, K. Marroquin and T. S. Teets, *Chem. Sci.*, 2019, **10**, 5124–5132.
4 F. Vögtle, M. Plevoets, M. Nieger, G. C. Azzellini, A. Credi, L. De Cola, V. De Marchis, M. Venturi and V. Balzani, *J. Am. Chem. Soc.*, 1999, **121**, 6290–6298.
5 G. M. Sheldrick, *Acta Crystallogr. Sect. C Struct. Chem.*, 2015, **71**, 3–8.
6 A. L. Spek, *Acta Crystallogr. D Biol. Crystallogr.*, 2009, **65**, 148–155.
7 C. Jiang and T. S. Teets, *Inorg. Chem.*, 2022, **61**, 8788–8796.